

Figure 4.1 Picard plot for the Shaw problem of Example 4.1.

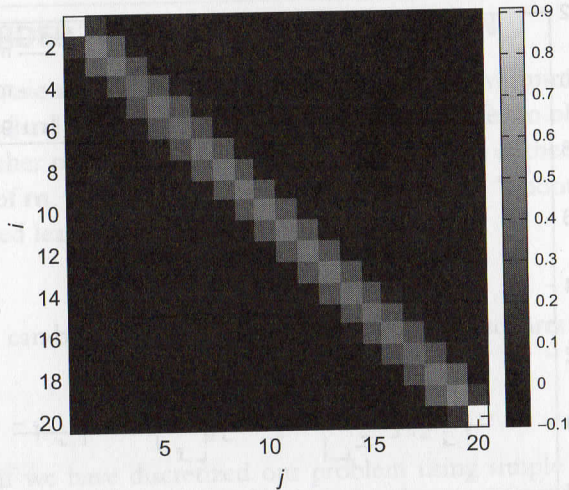


Figure 4.8 Resolution matrix for the Shaw problem, $\alpha = 4.29 \times 10^{-5}$. Note that the noise-free inversion of a spike model e_i will produce the i th column or row of \mathbf{R}_m (e.g., Figure 4.7 is a plot of the 10th column/row).

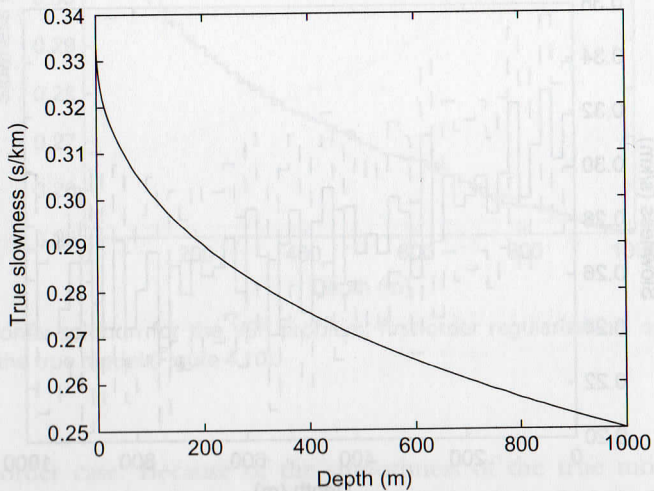


Figure 4.10 A smooth test model for the VSP problem.

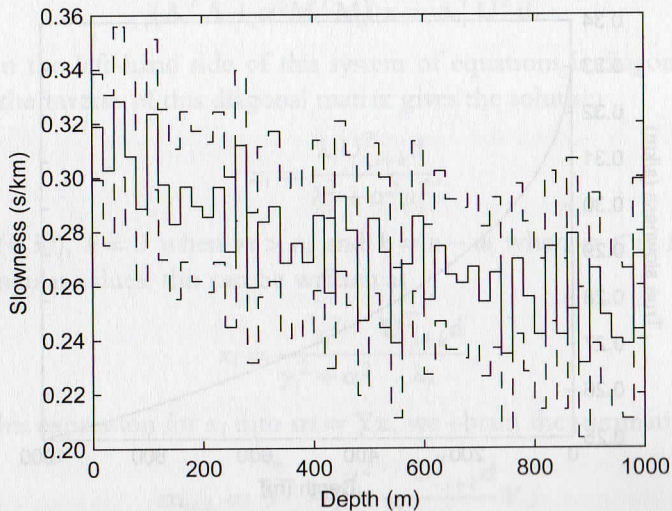


Figure 4.11 Least squares solution for the VSP problem, with 95% confidence intervals.

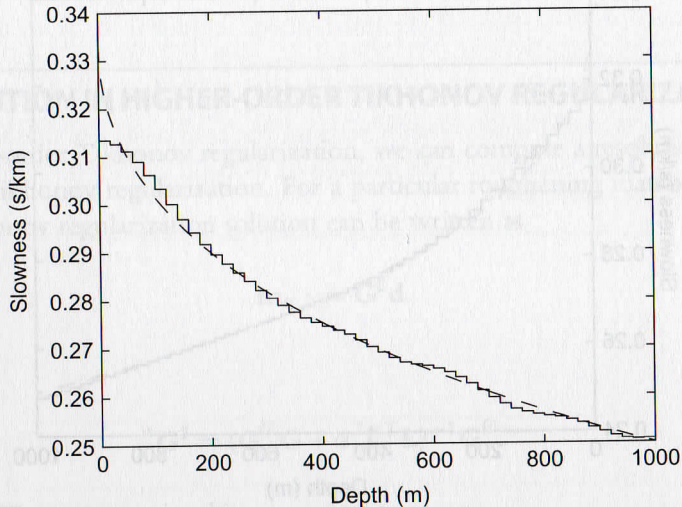


Figure 4.13 Tikhonov solution for the VSP problem, first-order regularization, $\alpha = 122$, shown in comparison with the true model (Figure 4.10).

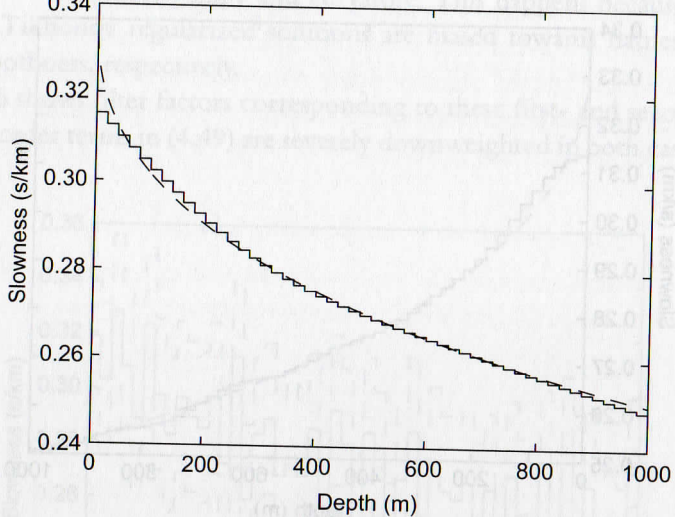


Figure 4.15 Tikhonov solution for the VSP problem, second-order regularization, $\alpha = 2341$, shown in comparison with the true model (Figure 4.10).

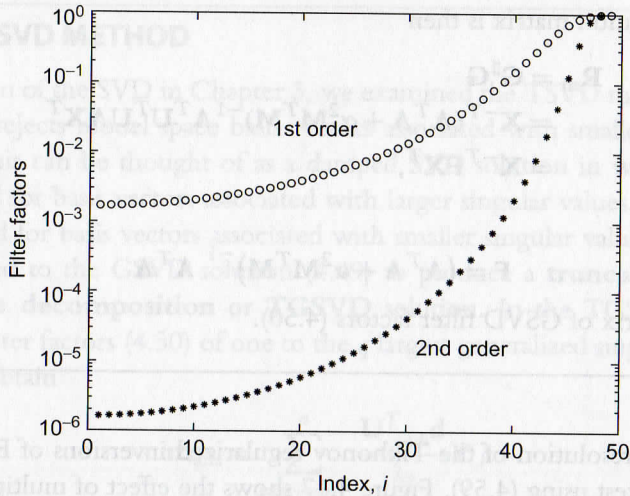


Figure 4.16 Filter factors (4.17) for optimal first- and second-order Tikhonov solutions to the VSP problem shown in Figures 4.13 and 4.15.

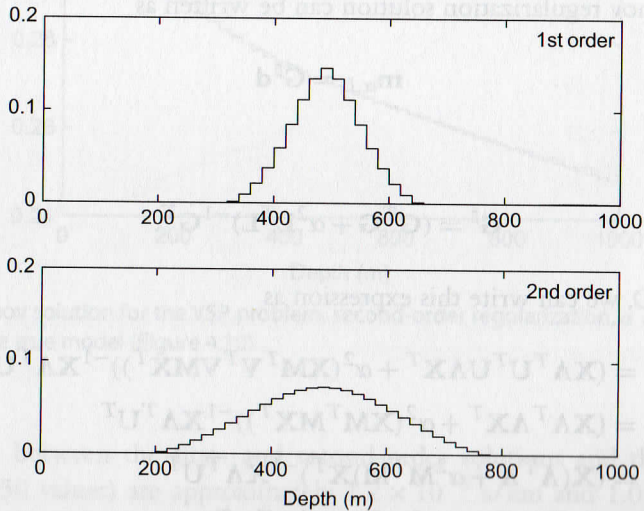


Figure 4.17 The model resolution matrix \mathbf{R}_m multiplied times the spike model for the first- and second-order regularized solutions of Example 4.4.

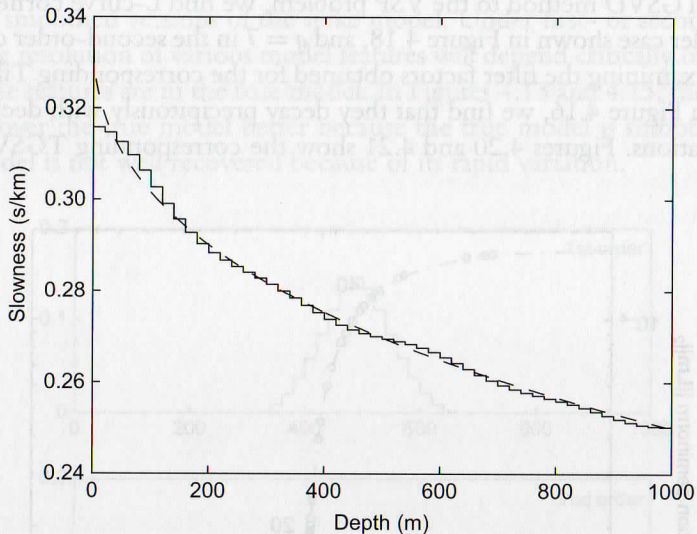


Figure 4.20 TGSVD solution of the VSP problem, $q = 8$, first-order regularization, shown in comparison with the true model.

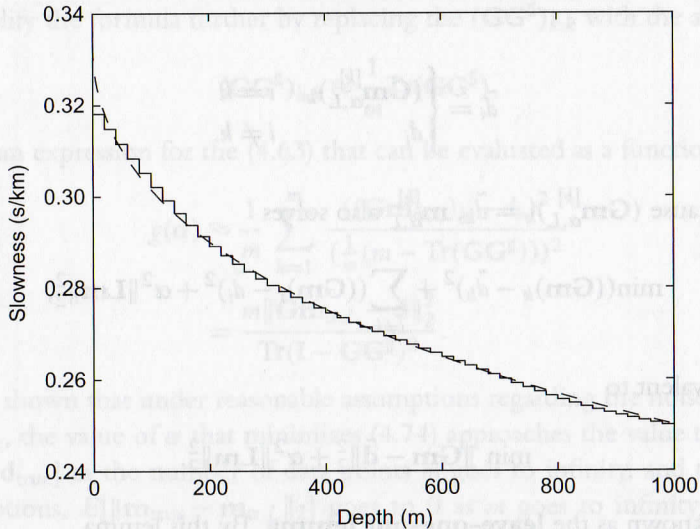


Figure 4.21 TGSVD solution of the VSP problem, $q = 7$, second-order regularization.

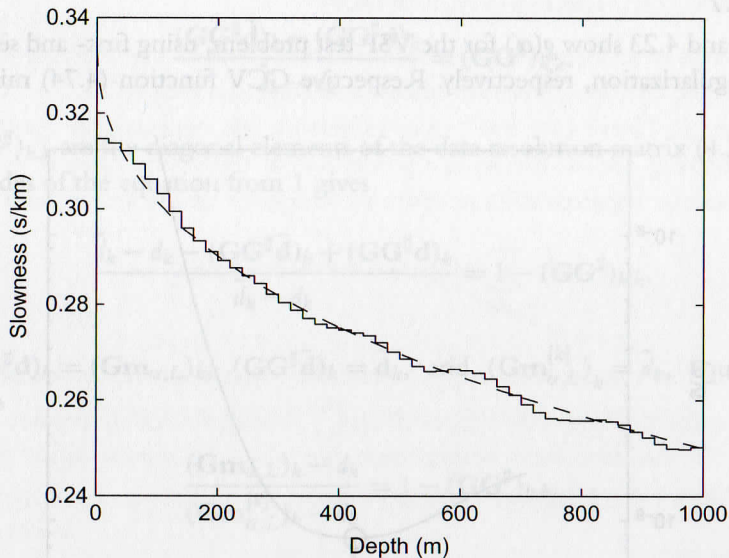


Figure 4.24 GCV solution for the VSP problem, first-order, $\alpha = 76.3$, shown in comparison with the true model.

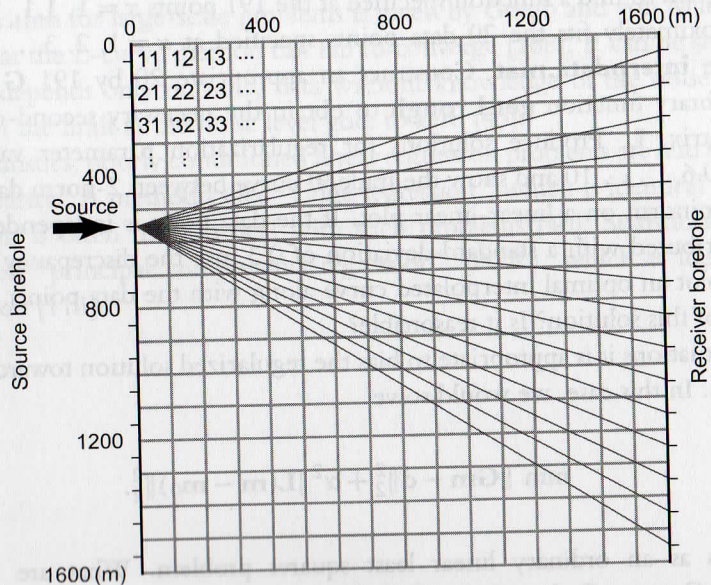


Figure 4.28 Cross-well tomography problem, showing block discretization, block numbering convention, and one set of straight source-receiver ray paths.